

## ***Technical Note***

## Downburst versus boundary layer induced wind loads for tall buildings

Jongdae Kim<sup>†</sup>, Horia Hangan<sup>‡</sup> and T.C. Eric Ho<sup>‡†</sup>

*Alan G Davenport Wind Engineering Group,  
The University of Western Ontario, London, Ontario, Canada  
(Received February 1, 2007, Accepted September 9, 2007)*

**Abstract.** Downbursts are transient phenomena that produce wind profiles that are distinctly different from synoptic boundary layers. Wind field data from Computational Fluid Dynamics (CFD) simulations of isolated downburst-like impinging jets, are used to investigate structural loads of tall buildings due to these high intensity winds. The base shear forces and base moments of tall buildings of heights between 120 and 250 m produced by downburst winds of various scales are compared with the forces from the equivalent boundary layer gust winds, with matched 10-metre wind velocity. The wind profiles are mainly functions of the size of the downburst and the radial distance from the centre of the storm. Wind forces due to various downburst profiles are investigated by placing the building at different locations relative to the storm center as well as varying the size of the downburst. Overall it is found that downbursts larger than approx. 2,000 m in diameter might produce governing design wind loads above those from corresponding boundary layer winds for tall buildings.

**Keywords:** downbursts; boundary layers; structural loads; tall buildings.

---

### 1. Introduction

Downburst winds are characterized as columns of cold air descending suddenly from the thunderstorm cloud base and impinging on the ground. These high intensity wind events are responsible for damage to many buildings and structures. In order to understand the complex flow dynamics of downbursts several generic experimental studies were conducted on wall jets (Bakke 1957, Poreh, *et al.* 1967) and impinging jets (Donaldson and Snedeker 1971, Didden and Ho 1985, Landreth and Adrian 1990, Cooper, *et al.* 1993, Chay and Letchford 2002, Letchford and Illidge 1999). Numerical atmospheric (Proctor 1988) and engineering simulations (Selvam and Holmes 1992, Wood, *et al.* 2001, Sengupta, *et al.* 2001) of downbursts were performed showing steady state and mean characteristics of the flow properties. Theoretical and empirical models (Zhu and Etkin 1985, Holmes and Oliver 2000) were also proposed for practical design use. Most empirical models are based on the mean wind speed profile with maximum wind speed close to the ground.

In a recent paper (Kim and Hangan 2007), time dependent simulations of downburst-like

---

<sup>†</sup> Research Engineer, E-mail: [jdk@blwtl.uwo.ca](mailto:jdk@blwtl.uwo.ca)

<sup>‡</sup> Assoc. Professor and Research Director, Corresponding Author, E-mail: [hmh@blwtl.uwo.ca](mailto:hmh@blwtl.uwo.ca)

<sup>‡†</sup> Research Director, E-mail: [ericho@blwtl.uwo.ca](mailto:ericho@blwtl.uwo.ca)

impinging jets were presented. It was shown that the highest horizontal wind speeds after impingement are produced by the interaction of shear layer produced ring-vortices and the unsteady separation-reattachment of the surface layer, generated just after these vortices touch down. The velocity profiles of a downburst-like impinging jet are time and space dependent, and differ qualitatively from those from boundary layer flows. Maximum velocities are reached between 1 and  $1.5 D_{jet}$  (jet-diameter) radial distance from the centerline of the jet and at a height of approximately  $z_{max}=0.05 D_{jet}$  from the ground (Kim and Hangan 2007).

Herein the results of the aforementioned spatio-temporal CFD model are used to determine quasi-steady wind loads due to downburst-like winds on typical tall buildings.

Most meteorological records are taken at about 10m height and they are often used as the basis for the derivation of wind speed specifications in wind codes. It is, however, not straightforward to uniquely identify downburst winds or boundary layer winds from the wind records. From some records, thunderstorm winds may be correlated to records of thunderdays. However, there is no indication in the meteorological records to relate these potential thunderstorm or downburst winds to the size of the storms.

Because of the fundamental difference in the wind profiles between downburst winds and boundary layer winds, a tall building may be subject to very different wind forces depending on the type of winds acting on it, given only the gust wind speed at 10 m. It is therefore instructive to determine the potential difference in wind-induced loads if the sources of these high wind speeds are unknown. In addition, the wind velocity profiles in downburst winds can vary significantly at different distances relative to the location of the storm, as well as a function of the size of the storm.

Assuming that the macro-flow dynamics is similar in both impinging jets and full scale downbursts, unsteady velocity profiles from CFD results are converted to full scale wind velocities. Quasi-steady wind loads of a tall building from the downburst-like winds are compared with those from the equivalent boundary layer winds with matched 10-metre height wind velocity.

## 2. Flow field

### 2.1. Numerical simulations

In what follows the downburst CFD simulation data previously obtained (Kim and Hangan 2007) are used to determine the wind loads on typical tall buildings. The CFD modeling is detailed in (Kim and Hangan 2007) and therefore, for convenience, only the main features of that model are presented herein. The downburst-like impinging jet was modeled as an axisymmetric flow about the vertical axis. Fig. 1 shows the parameters related to the computational domain, the resulting radial velocity profile and the building. The time-dependent (unsteady) simulations were conducted using converged structured grids strenuously refined in the surface layer. A Reynolds Stress Model (RSM) with wall reflection terms, a second order implicit time discretization and a SIMPLEC scheme for the pressure-velocity coupling were employed.

The flow was found to be Reynolds number dependent at low Reynolds numbers (below 15,000) and in the surface layer only, (Xu and Hangan 2005). Therefore the simulations corresponding to  $Re=20,000$  (based on jet diameter and jet velocity) are used herein.

The height of the impinging-jet above the ground,  $Z_{jet}$ , is a generic indicator of the height of the thunderstorm base-cloud above the ground. To investigate the effects of this height above the ground, three cases of downburst characteristics are attempted corresponding to  $Z_{jet}/D_{jet}=1, 2$  and 4.

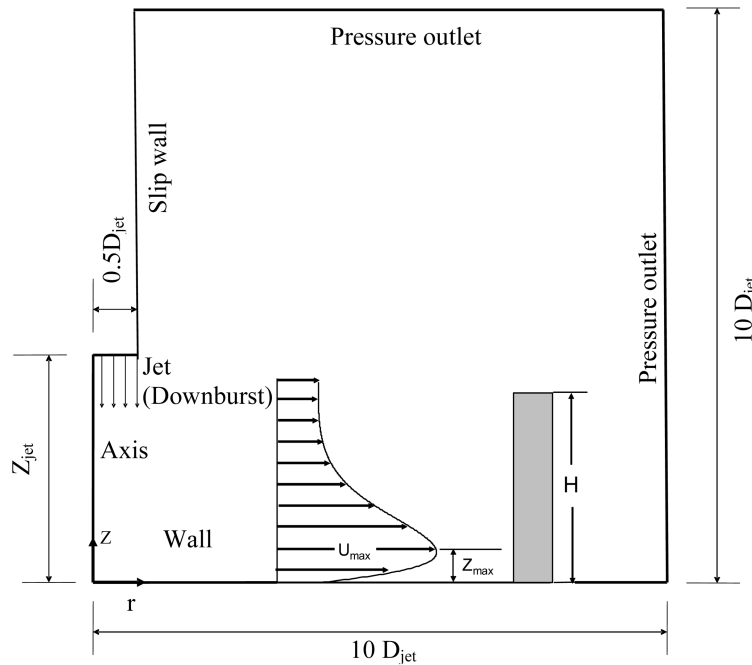


Fig. 1 Schematic diagram of computational domain and main parameters

The maximum radial velocities were observed at  $r/D_{jet}=1.1$ , 1.2 and 1.4 corresponding to these three  $Z_{jet}/D_{jet}$  cases. Fig. 2 shows the time evolutions of normalized radial velocities computed at these radial locations and at a fixed height of  $z/D_{jet}=0.02$ . For a microburst with a diameter  $D_{jet}=500$  m, this corresponds to the standard 10-metre height commonly used to specify reference wind speed.

## 2.2. Wind profiles

The radial velocity profiles from the numerical simulations are converted to full scale downburst wind profiles by employing scale factors to obtain full scale conditions of  $V_{jet} = 50$  m/s and  $D_{jet} = 500 \sim 3000$  m. In Figs. 3 to 5, the downburst wind velocity profiles of various jet diameters are compared with a typical open exposure boundary layer gust wind profile (power law exponent=0.11) with identical 10m height speed ( $V_{10}$ ). In these cases, the downburst profile is taken at the time when the maximum radial velocity is reached. The three cases presented correspond to the three maximum radial velocity situations, Case I, II and III, in Fig. 2.

It is clear that the downburst wind profiles are not universal and depend on the radial distance,  $r$ , from the centre of the storm and the size of the downburst jet,  $D_{jet}$ . As the downburst size increases, the vertical location of maximum wind speed,  $z_{max}$ , moves upwards. As well, the “bulge” with the maximum wind speed extends to be an almost uniform high speed region over a significant range of height. This has a strong implication for tall buildings as, in the case of a large downburst, most of the building height will be within this range of high wind speed. Overall this happens for downburst diameters  $D_{jet} > 1,500$  m. For example, at  $D_{jet}=3000$  m, the wind speed resulting from the downburst is larger than that from the boundary layer between 10m height and the top of the tall buildings considered herein.

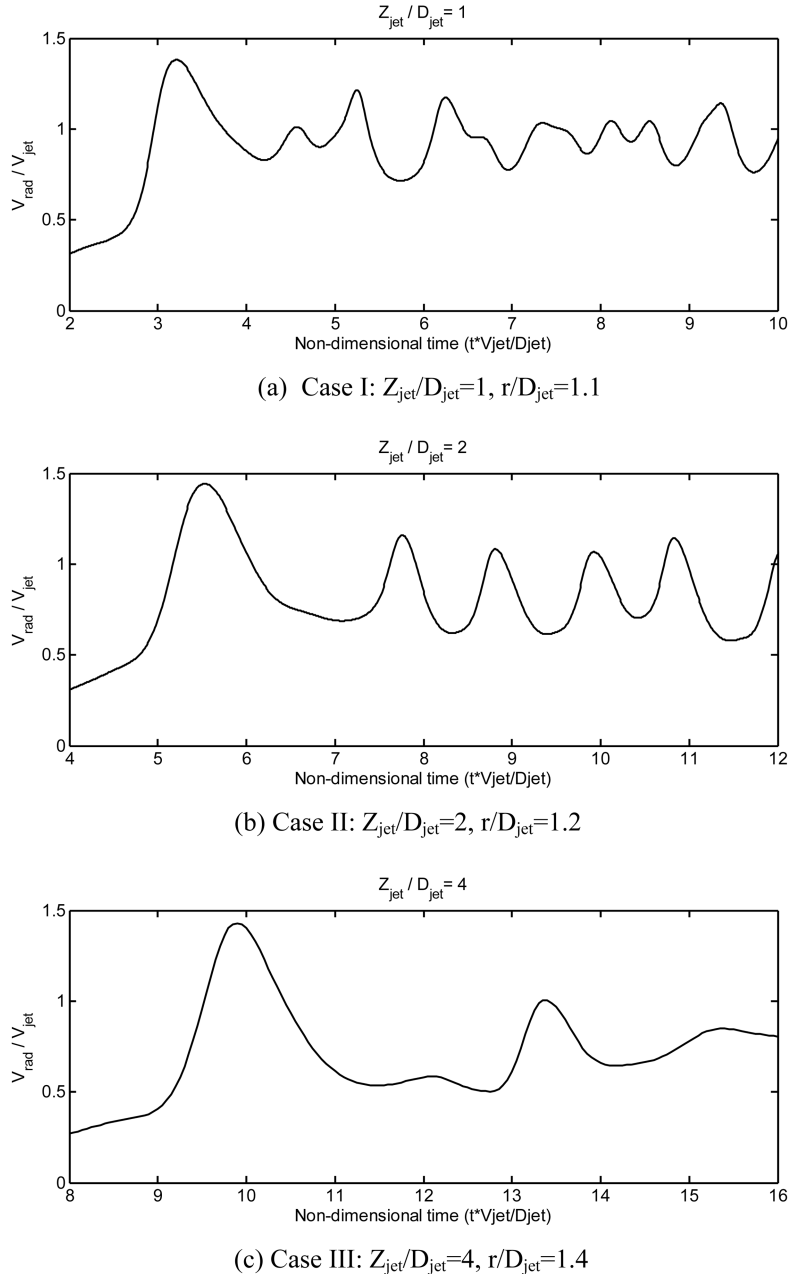


Fig. 2 Normalized radial velocity measured at height of  $z/D_{jet}=0.02$  for various jet-to-surface distances,  $Z_{jet}/D_{jet} = 1, 2$  and  $4$ .

### 3. Structural loads

The structural effects of downburst winds is investigated by calculating the maximum quasi-steady wind loads (base shears and base moments) at any moment in time on three typical tall

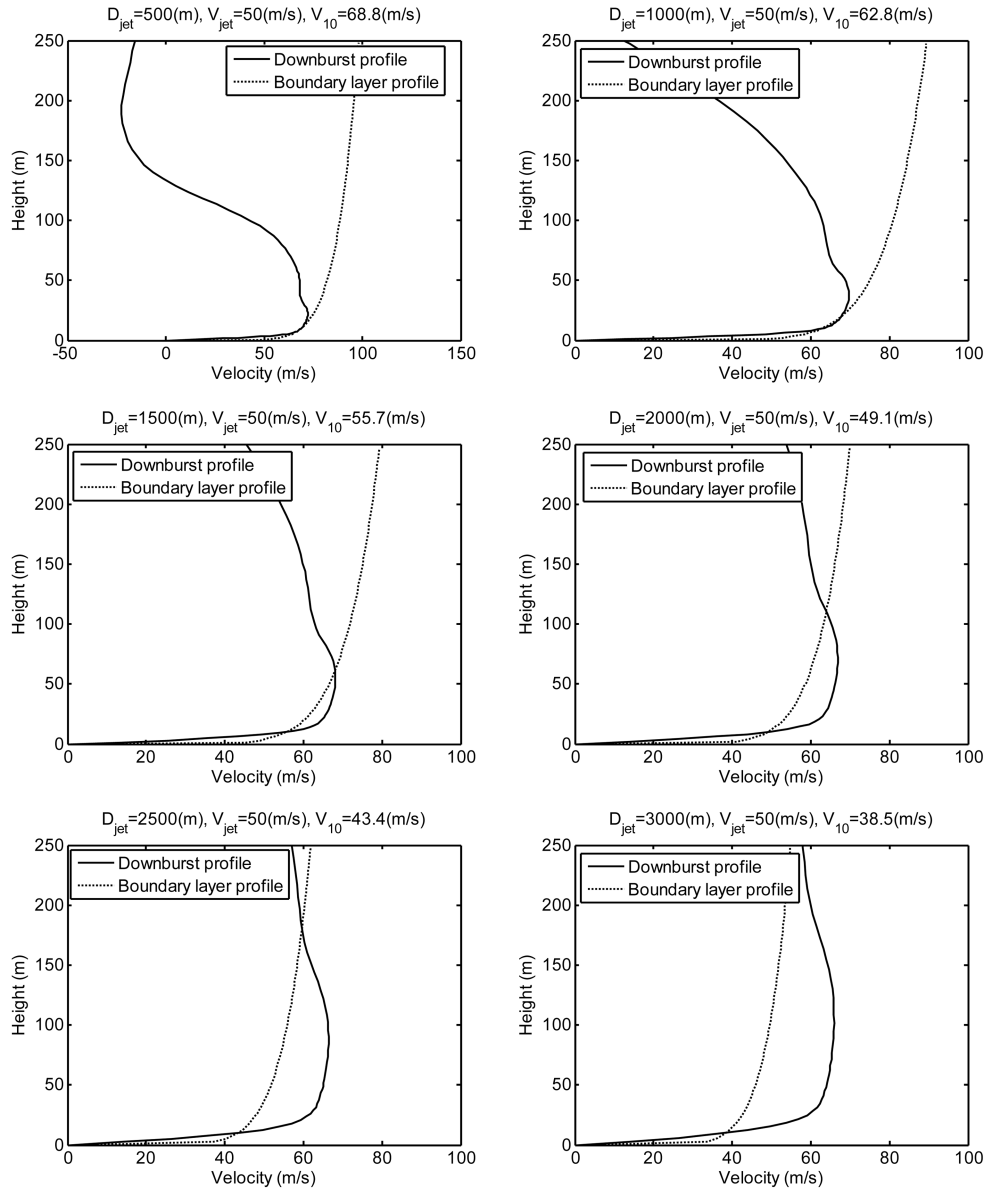


Fig. 3 Downburst and boundary layer wind velocity profiles (wind speed matched at  $z = 10$  m) measured at  $r/D_{jet} = 1.1$  for Case I:  $V_{jet} = 50$  m/s,  $Z_{jet}/D_{jet} = 1$

buildings of heights,  $H = 120$ m,  $H = 183$  m and  $H = 250$  m.

While the simulated downburst winds are time dependent, see Fig. 2 and (Kim and Hangan 2007), the frequency associated with their quasi-periodic variation is small (due to limitations in the RANS simulations) compared to typical natural frequencies of tall buildings and therefore only quasi-static loads are calculated herein. However, these loads are calculated for downburst profiles at every time step of the CFD simulations, and the maximum responses over the entire duration are then extracted. Recent studies of full scale downburst records (Holmes, *et al.* 2007a, Holmes, *et al.*

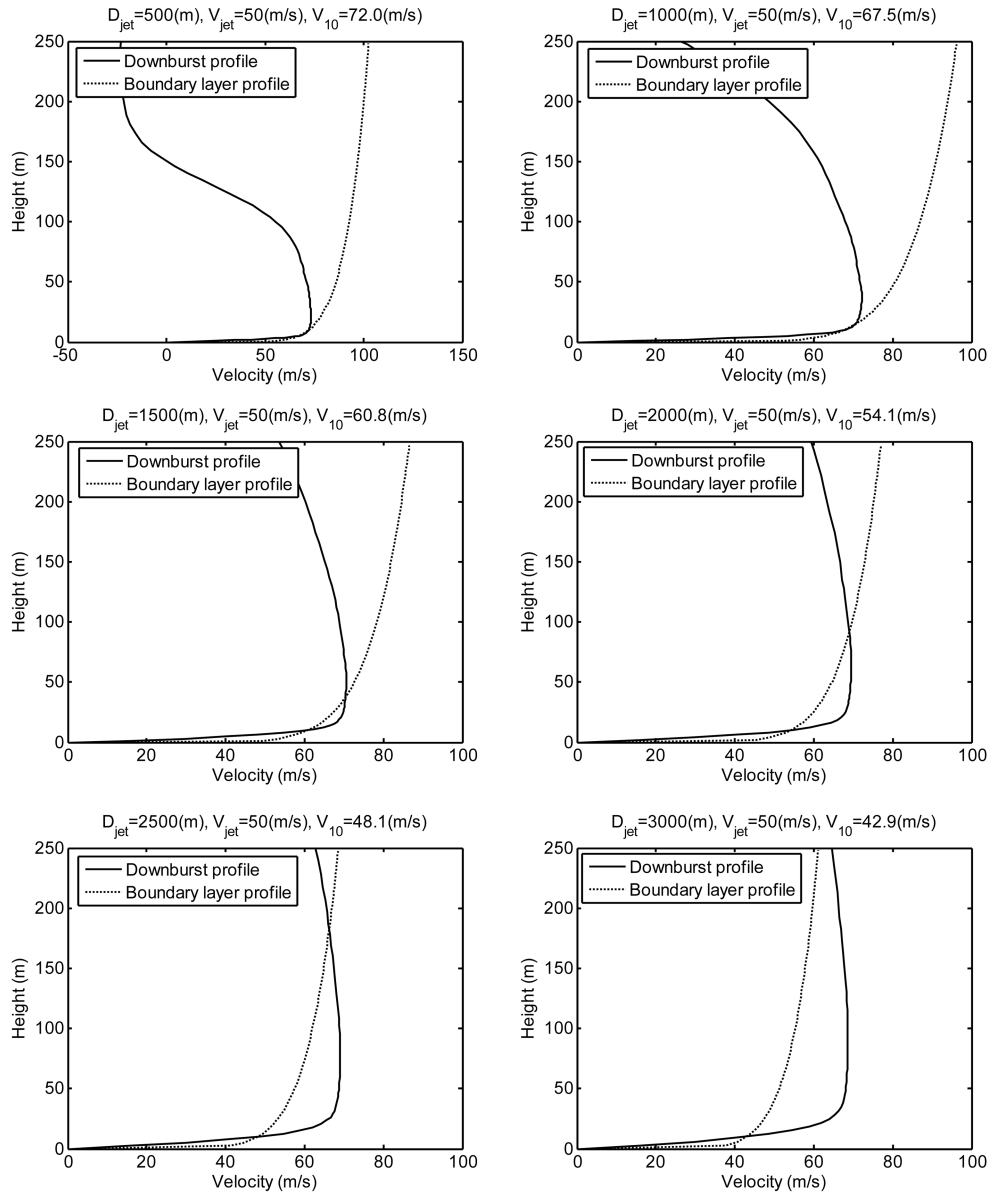


Fig. 4 Downburst and boundary layer wind velocity profiles (wind speed matched at  $z = 10$  m) measured at  $r/D_{jet} = 1.2$  for Case II:  $V_{jet} = 50$  m/s,  $Z_{jet}/D_{jet} = 2$

2007b), suggest that the non-stationary turbulence characteristics of the downburst winds may be similar to the equivalent stationary turbulence characteristics of the boundary layer wind. Also, little information is available on the distribution of the turbulent energy in the frequency domain of downburst winds, (Holmes, *et al.* 2007b). As a first indicator of the effect of the wind profiles, resonance-induced inertia loads are ignored and quasi-static wind loads are used for comparison.

At every time step of the CFD simulation the wind-induced structural responses, base shear (BS) and base moment (BM) are calculated as follows:

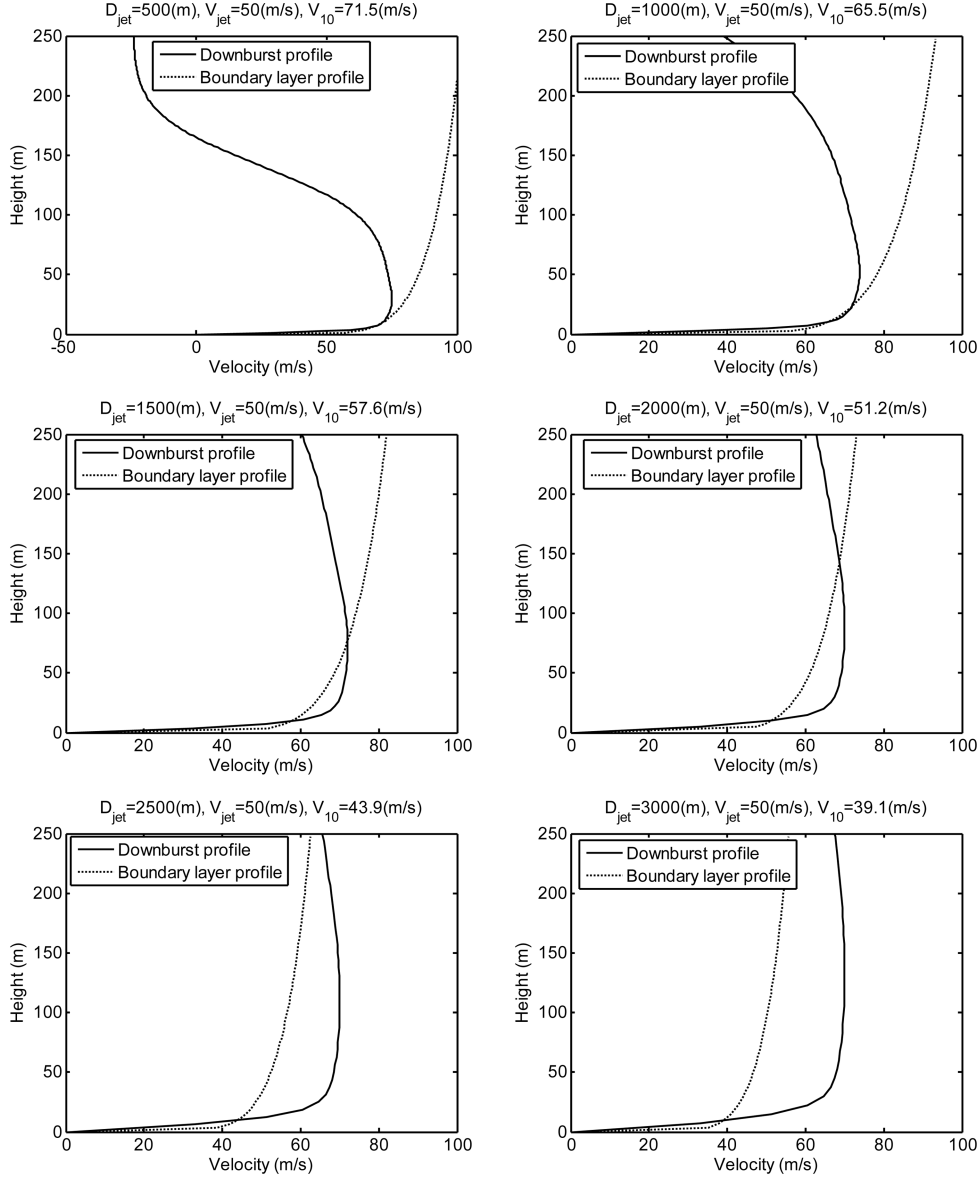


Fig. 5 Downburst and boundary layer wind velocity profiles (wind speed matched at  $z=10$  m) measured at  $r/D_{jet} = 1.4$  for Case III:  $V_{jet}=50$  m/s,  $Z_{jet}/D_{jet}=4$

$$BS(t) = \int_0^H f(z, t) dz \tag{1}$$

$$BM(t) = \int_0^H f(z, t) z dz \tag{2}$$

where,  $H$  : building height,

$f(z, t) = 0.5 \rho_{air} v^2(z, t) C_D(z) B(z)$  : wind force at height  $z$

$\rho_{air}$  : air density

$v(z, t)$  : wind speed at  $z$

$C_D(z)$  : drag coefficient at  $z$

$B(z)$  : building width at  $z$

Three buildings of different heights,  $H=120, 183$  and  $250$  m, are used to compare the effects of downburst and boundary layer winds on structural responses. The three buildings have the same rectangular plan dimensions of  $45\text{m}$  and  $30\text{m}$ . The building of height  $H=183$  m corresponds to the Commonwealth Aeronautical Advisory Research Council (CAARC) standard tall building (Holmes, *et al.* 1989) previously used for comparison of wind tunnel results among different laboratories.

Wind loads of each building were calculated by changing the downburst size ( $D_{jet}=500\sim 3500$  m) and by locating the building at different radial distances from the downburst centre ( $r/D_{jet}=0$ ) to a maximum of  $r/D_{jet}=3$ . During a downburst event, the maximum base shear and base moment were calculated for each time. These loads were then normalized by their maximum value over all downburst diameters (*maximum maximorum*), and are presented relative to downburst diameters in Figs. 6, 7 and 8. The base shears and base moments were determined for the three building heights, Fig. 6 (a), (b), (c) and Fig. 7 (a), (b), (c), respectively. Moreover, every plot presents the critical cases corresponding to the three downburst jet-to-ground positions:  $z/D_{jet}=1$  (Case I),  $z/D_{jet}=2$  (Case II) and  $z/D_{jet}=4$  (Case III).

As building heights increase, the downburst size that induces maximum structural loads also

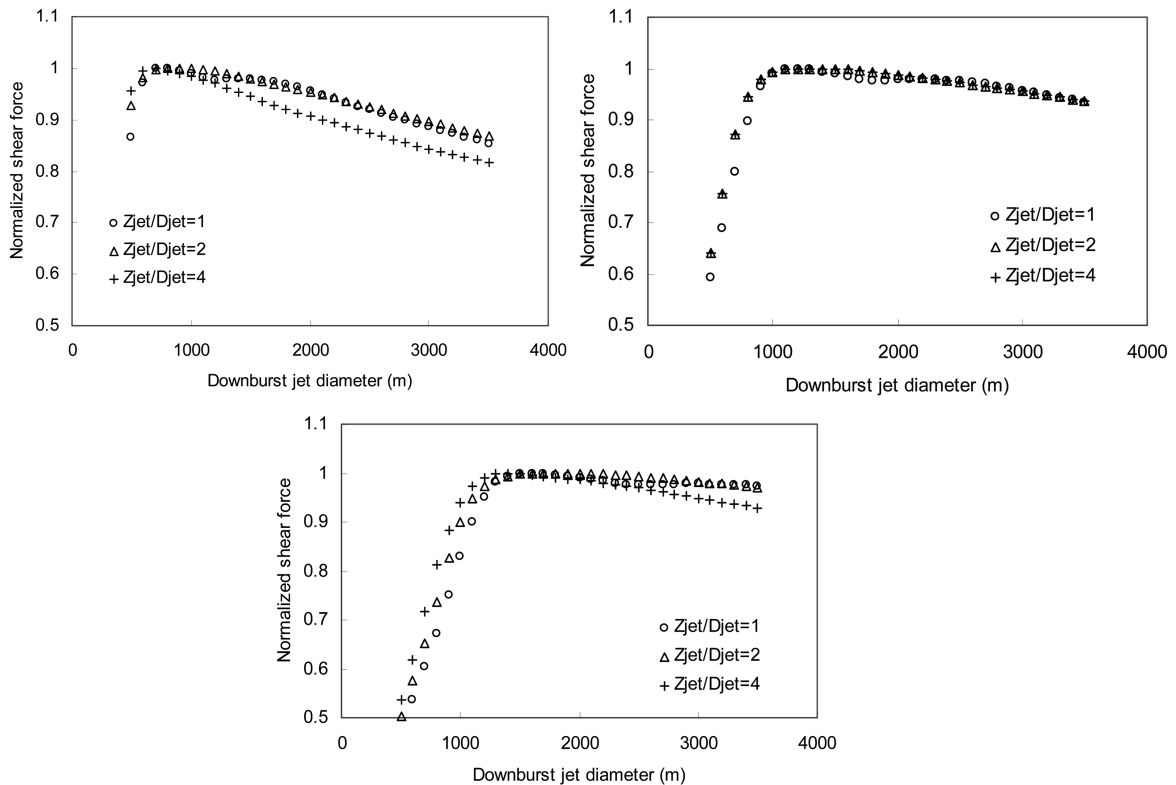


Fig. 6 Normalized shear force for building heights: a)  $H=120$  m, b)  $H=183$  m and c)  $H=250$  m Maximum shear forces are calculated over a radial range of  $r/D_{jet}=0.1\sim 3$ . These maximum shear forces are then normalized by their maximum maximum value over the range of  $D_{jet}=500\sim 3500$  m

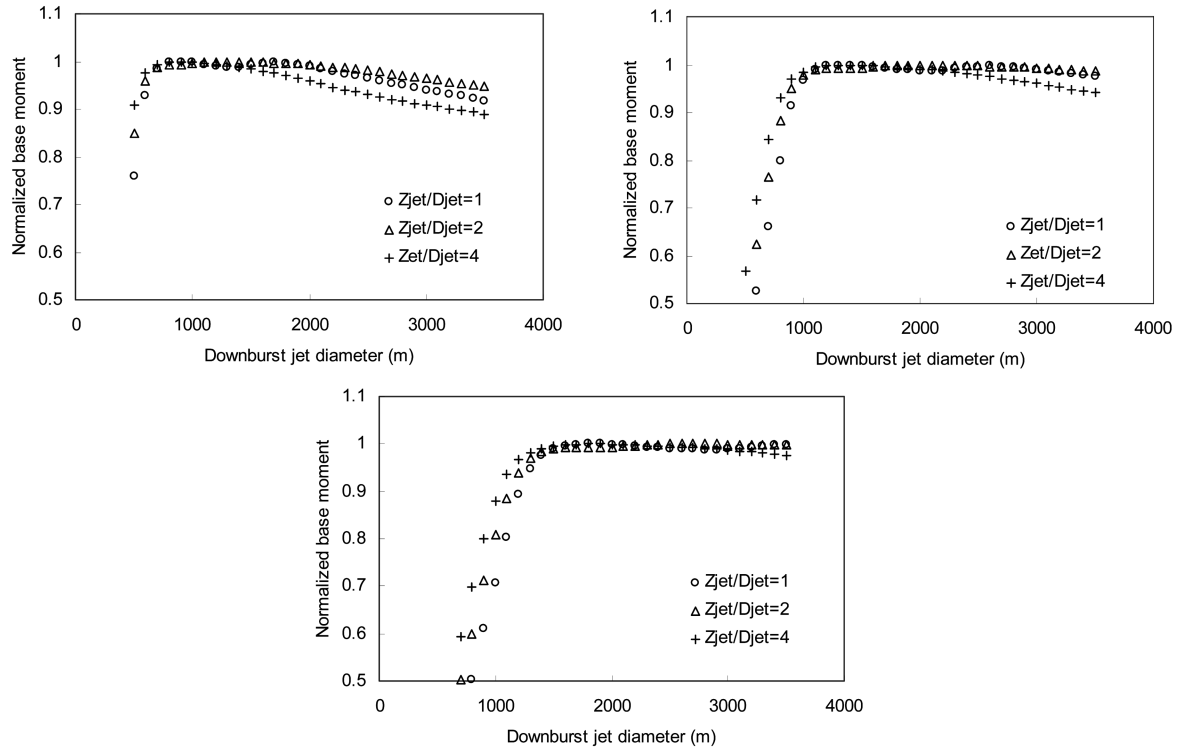


Fig. 7 Normalized base moment for building heights: a)  $H=120$  m, b)  $H=183$  m and c)  $H=250$  m Maximum base moments are calculated over a radial range of  $r/D_{jet} = 0.1-3$ . These maximum base moments are then normalized by their maximum maximum value over the range of  $D_{jet} = 500-3500$  m

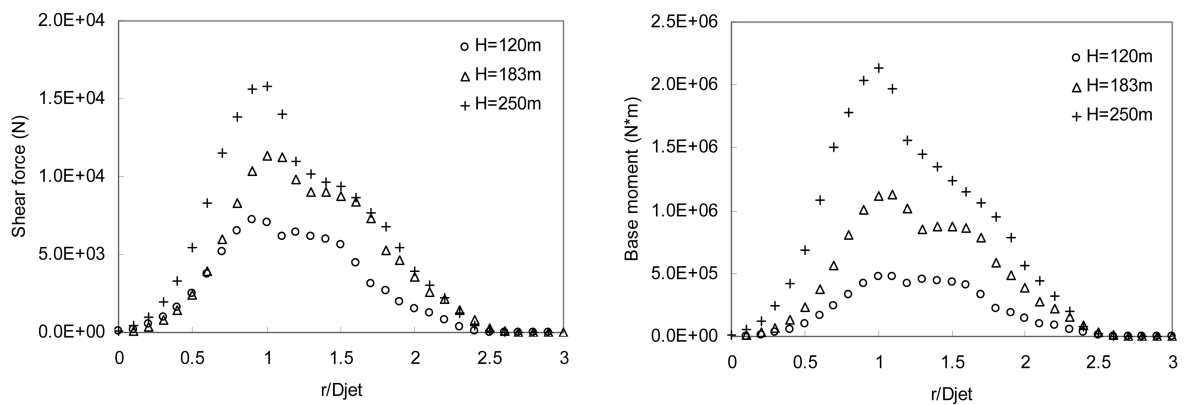


Fig. 8 Variation of base shear force and moment with radial location of the building, for  $Z_{jet}/D_{jet}=1$ ,  $D_{jet}=2000$  m

increases. After reaching a maximum value, the normalized loads show a slight decay or a quasi-asymptotic behavior with further increase in downburst diameter. The normalizing maximum values closely correspond to downburst jet diameters  $D_{jet} \cong 2,000$  m.

To demonstrate the importance of the radial positions of the building from the downburst jet

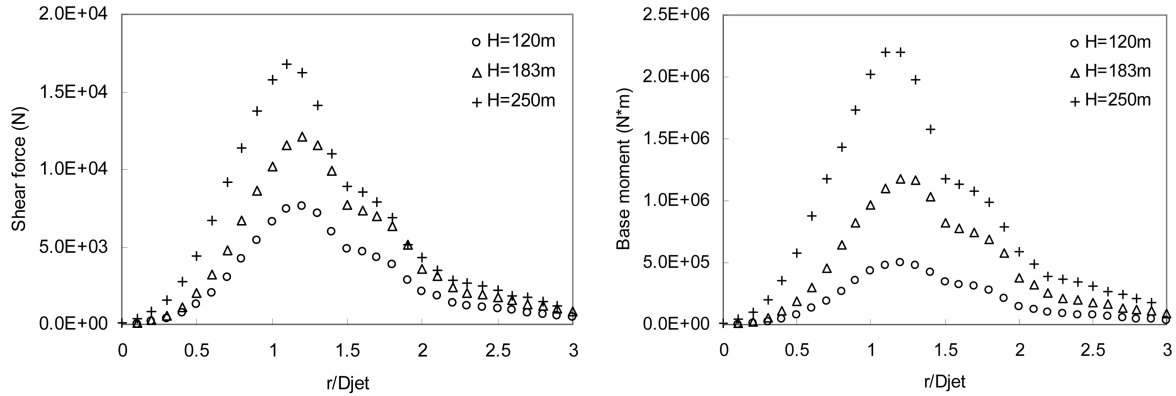


Fig. 9 Variation of base shear force and moment with radial location of the building, for  $Z_{jet}/D_{jet}=2$ ,  $D_{jet}=2000$  m

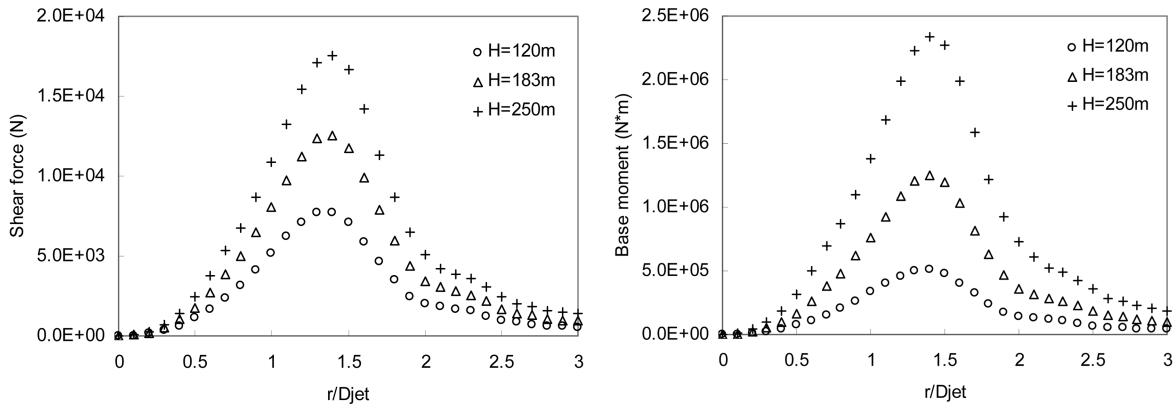


Fig. 10 Variation of base shear force and moment with radial location of the building, for  $Z_{jet}/D_{jet}=4$ ,  $D_{jet}=2000$  m

center, the maximum base shears and moments at different radial positions are calculated and plotted in Fig. 8, 9, and 10 for  $D_{jet} = 2,000$  m. Again, the base shear and moment results are presented for the three building heights.

For Case I, Fig. 8, ( $Z_{jet}/D_{jet}=1$ ), all loads reach maximum values for  $r/D_{jet}=1.1$ . For Case II, Fig. 9, and III, Fig. 10, as  $Z_{jet}/D_{jet}$  increases, maximum loads occur at  $r/D_{jet}=1.2$  and  $1.4$ , respectively. Overall, as expected, the maximum loads are reached at radial distances corresponding to maximum radial velocities, see Fig. 2.

As the relative downburst jet height,  $Z_{jet}/D_{jet}$ , increases, the thickness of the shear layer increases (similar to free jet flows) until the initial ring vortex touches the ground. As the ring vortex, formed at the downburst jet outflow, approaches the ground, its size also increases. After touching down, the ring vortex convects radially and triggers the surface layer separation-reattachment, (Kim and Hangan 2007). The stretching of the flow between the primary vortex and the separation-reattachment bubble produces the highest wind speeds. The location and strength of this high wind speed region depends on the size of the primary vortex. This is reflected in Figs. 8, 9 and 10: with increasing downburst-to-ground distance,  $Z_{jet}/D_{jet}$ , the maximum loads increase, as their corres-

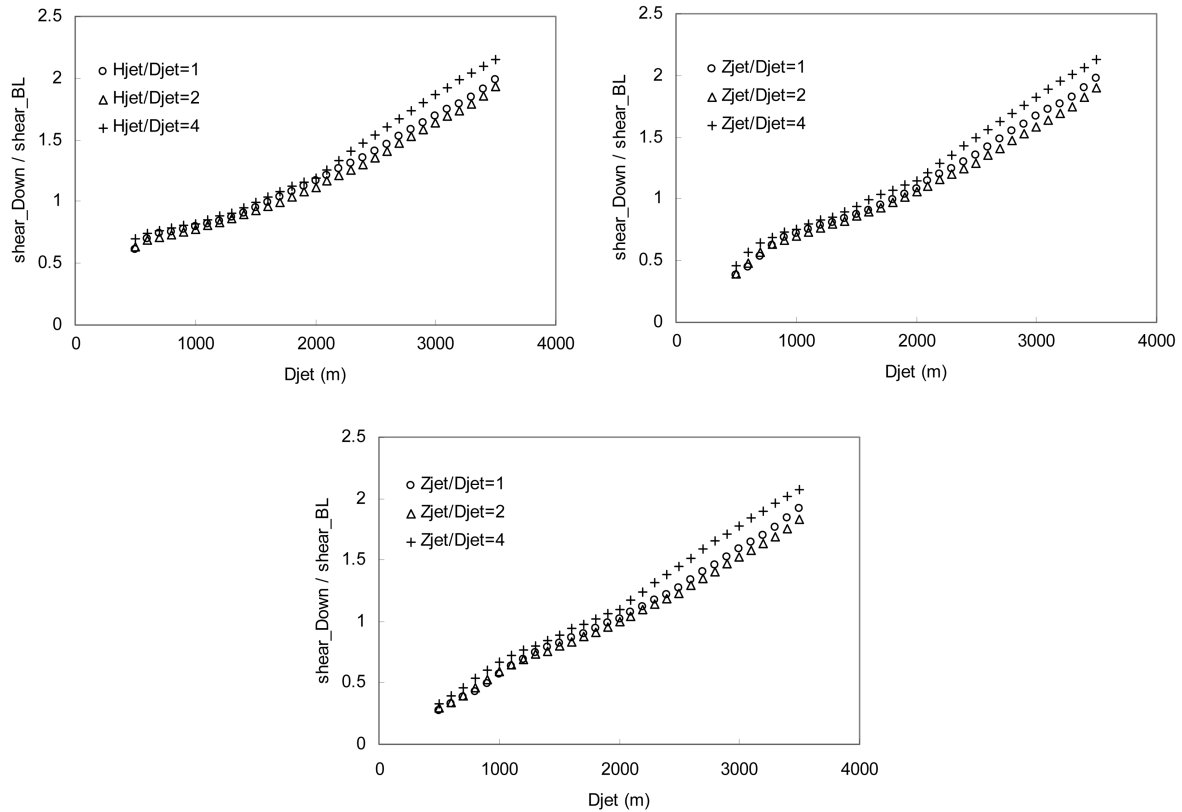


Fig. 11 Base shear force ratio (base shear from downburst / base shear from boundary layer wind) as function of downburst-jet diameter: a)  $H = 120$  m, b)  $H = 183$  m, c)  $H = 250$  m

ponding radial location moves radially outward.

Figs. 11 and 12 show the ratio between structural loads produced by downburst and boundary layer winds. First, structural loads were calculated for every time increment that a downburst wind speed is given from the CFD simulation, using the instantaneous downburst wind profile. At each corresponding time increment, structural loads were also calculated using a boundary layer profile with matched gust wind speed at 10-meter height. The maximum quasi-static loads over the entire storm duration are then extracted and ratios of the maximums were calculated with the boundary layer loads as the base. The results are represented in Fig. 11 and 12. Ratios above 1 signify that the downburst loading is larger than the corresponding loading from (10 m height matched) boundary layer winds.

For a building of  $H = 120$  m, the critical downburst size is around  $D_{jet} = 1700$  m. Above this critical size, downburst winds become dominant over boundary layer winds in terms of structural loads. For buildings of  $H = 183$  m and 250 m, the critical downburst size is around  $D_{jet} = 2000$  m. Considering the average size of observed downbursts (Hjelmfelt 1988) between 1500 and 3000 m, downbursts may become the dominant winds for structural responses of tall buildings.

However, note that this is a quasi-steady approach and for tall buildings the dynamic effects are also important. It is expected that since the boundary layer winds from synoptic storm systems last longer (hours) the chance of reaching a peak is increased compared to thunderstorm generated downburst events (few minutes in duration).

#### 4. Conclusions

The wind fields generated by previous CFD simulations of downburst-like impinging jets were applied to estimate the structural wind loads on tall buildings of various heights. The CFD generated wind fields were scaled to simulate various downburst outflow diameters  $D_{jet}=500\sim 3,500$  m for an outflow velocity  $V_{jet}=50$  m/s. Wind loads on tall buildings of various heights were then calculated using the simulated downburst winds, and compared with loads calculated from boundary layer winds with matched 10-meter wind speeds. For every downburst diameter considered, the building radial position as well as the height of the downburst outflow above ground was varied.

Downburst induced structural loads were found to vary significantly depending on the relative radial position of the building to the storm centre, in correlation with the radial variation of the velocity profiles. As the distance between the downburst outflow and the ground increases, the dimension of the main ring vortices increases. This translates into larger magnitudes and outer radial positions of maximum responses.

Based on Figs. 11 and 12 a parametric space for design may be visualized. In Fig. 13 the building heights are plotted versus critical downburst diameters, for which both the shear and the base moment ratios exceed 1, i.e., downburst wind loads exceed boundary layer wind loads. Design cases on the left side of the lines (zone I) correspond to boundary layer winds being dominant. Design

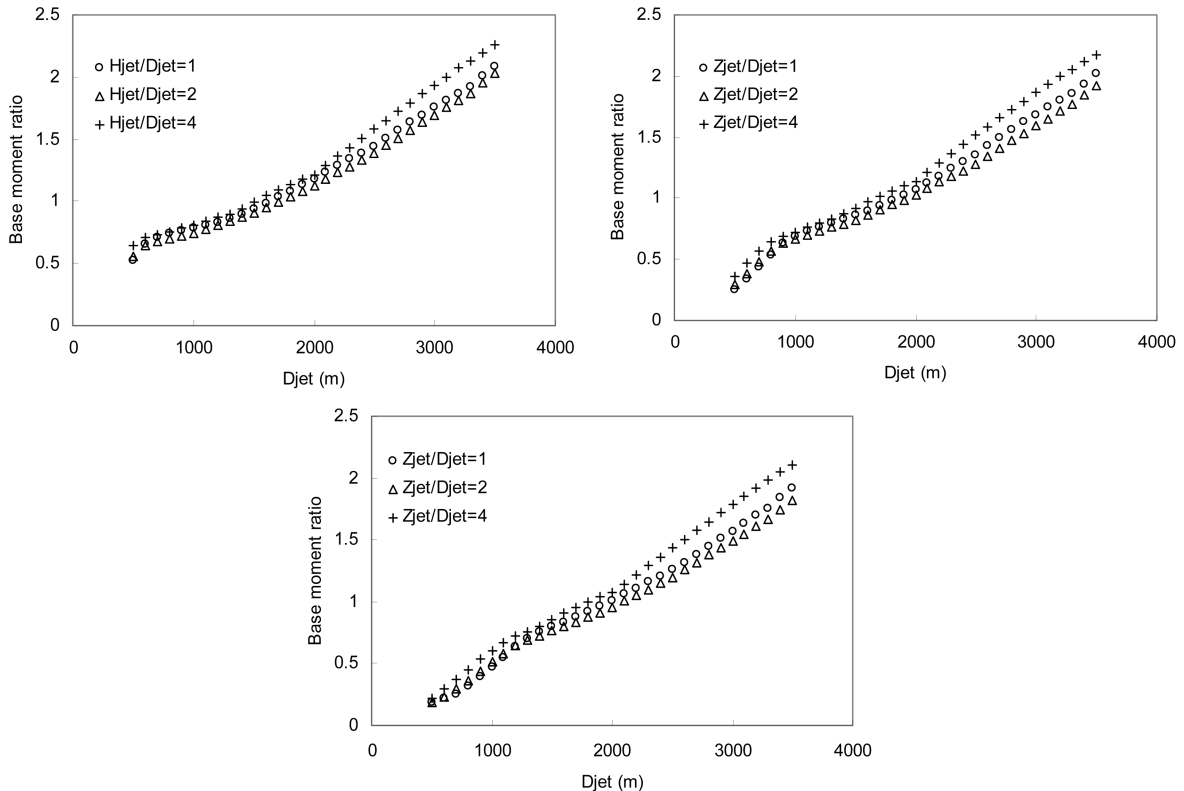


Fig. 12 Base moment ratio (base moment from downburst / base moment from boundary layer wind) as function of downburst-jet diameter: a)  $H=120$  m, b)  $H=183$  m, c)  $H=250$  m

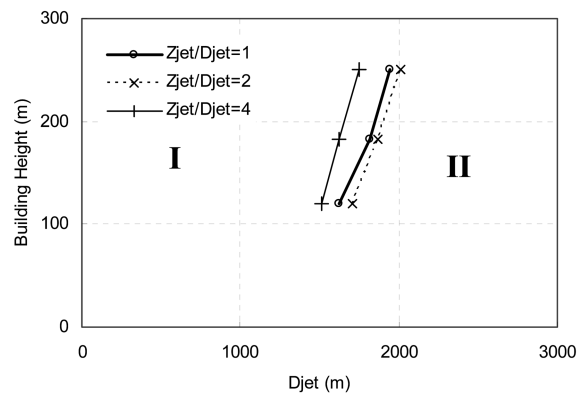


Fig. 13 Building heights vs. critical downburst jet diameter

cases on the right side (zone II) correspond to downburst events that may become structurally dominant over the boundary layer winds and may require further considerations. Suitable procedures should be developed in order to consider their effects.

Although the current investigation is based on quasi-steady loads, recent results (Holmes, *et al.* 2007b) suggest that the turbulence characteristics may have equivalent statistical properties as the boundary layer wind, giving a first indication of the range of building height classes that may be affected.

Furthermore, the present results are obtained based on CFD simulations using RANS models which reproduce only the large-scale flow dynamics coupled with a quasi-steady structural response analysis. Therefore further investigations on the effect of the storm duration on various structural load effects and the details of the turbulence characteristics of downburst winds are required before standard design procedure can be developed. Studies in thunderstorm, or downburst, wind climatology are also required to evaluate the relative risk due to this storm type and map design wind speeds for practical design use.

## Acknowledgements

This research has been made possible through funding from NSERC Industrial Collaborative Grant, ICLR Research Grant for High Intensity Winds Simulations and Manitoba Hydro funding. The authors also acknowledge the fruitful discussions with Dr. John Holmes on downburst winds and loading.

## References

- Bakke, P. (1957), "An experimental investigation of a wall jet", *J. Fluid Mech.*, **2**, 467–472.
- Chay, M.T. and Letchford C.W. (2002), "Pressure distributions on a cube in a simulated thunderstorm downburst –Part A: stationary downburst simulations", *J. Wind Eng. Ind. Aerod.*, **90**, 711-732.
- Cooper, D., Jackson, D.C., Launder, B.E. and Liao, G.X. (1993), "Impinging jet studies for turbulence model assessment - I. Flow fields experiments", *Int. J. Heat and Mass Transfer*, **36**, 2675-2684.
- Didden, N. and Ho C.M. (1985), "Unsteady separation in a boundary layer produced by an impinging jet", *J. Fluid Mech.*, **160**, 235-256.
- Donaldson, C. D. and Snedeker, R. S. (1971), "A study of free jet impingement, Part 1. Mean properties of free

- and impinging jets”, *J. Fluid Mech.*, **45**, 281-319.
- Hangan, H. and Xu, Z. (2005), “Scale, roughness and initial conditions effects in impinging jets with application to downburst simulations”, *10th Americas Conference on Wind Engineering, Baton Rouge, Louisiana, USA, May 31-June 4, 2005*.
- Hjelmfelt, M. R. (1988), “Structure and life cycle of microburst outflows observed in Colorado”, *J. Appl. Met.*, **27**, 900-927.
- Holmes, J.D., Melbourne, W.H. and Walker, G.R. (1989), “A commentary on the Australian Standard for wind loads”, AS 1170 Part 2, Australian Wind Engineering Society.
- Holmes, J.D. and Oliver, S.E. (2000), “An empirical model of a downburst”, *Eng. Str.* **22**, 1167-1172.
- Holmes, J.D., Hangan, H. and Schroeder, J. L. and Letchford, C. W. (2007a), “A forensic study of the Lubbock-Reese downdraft of 2002. II. Running-mean wind speeds and turbulence”, *12th International Conference on Wind Engineering and Industrial AerodynamicsICWEIA12, Cairns, Australia, July, 2007*.
- Holmes, J.D., Hangan, H. and Schroeder, J. L. and Letchford, C. W. (2007b), “A forensic study of the Lubbock-Reese downdraft of 2002. I. Storm characteristics”, *12th International Conference on Wind Engineering and Industrial AerodynamicsICWEIA12, Cairns, Australia, July, 2007*.
- Kim, J. and Hangan, H. (2007), “Numerical characterization of impinging jets with application to downbursts”, *J. Wind Eng. Ind. Aerodyn.*, **95**, 279-298.
- Landreth, C.C. and Adrian R.J. (1990), “Impingement of a low Reynolds number turbulent circular jet”, *Exp. Fluids*, **9**, 74-84.
- Letchford, C.W. and Illidge, G. (1999), “Turbulence and topographic effects in simulated thunderstorm downdrafts by wind tunnel jet”, *Proc: 10<sup>th</sup> International Conference on Wind Engineering, 21 - 25 June, Copenhagen, Balkema, Netherlands, 1907-1912*.
- Poreh, M., Tsuei, Y. G. and Cermak, J.E. (1967), “Investigation of a turbulent radial wall jet”, *ASME J. Appl. Mech.*, **34**, 457-463.
- Proctor, F. H., (1988), “Numerical simulations of an isolated microburst. Part I: dynamics and structure”, *J. Atmos. Sci.*, **45**, 3137-3160.
- Selvam, R. P. and Holmes, J.D. (1992), “Numerical simulation of thunderstorm downdrafts”, *J. Wind Eng. Ind. Aerodyn.*, **41-44**, 2817-2825.
- Sengupta, A., Sasrkar, P. P., and Rajagopalan, G. (2001), “Numerical and physical simulation of thunderstorm downdraft winds and their effects on buildings”, *Americas Conference on Wind Engineering-2001*.
- Wood, G.S., Kwok, K.C.S., Motteram, N.A. and Fletcher, D.F. (2001), “Physical and numerical modeling of thunderstorm downbursts”, *J. Wind Eng. Ind. Aerodyn.*, **89**, 535-552.
- Zhu, S. and Etkin, B. (1985), “Model of the wind field in a downburst”, *J. Aircraft*, **22**, 595-601.